INFRARED THERMOGRAPHY AND INVERSE PROBLEM ANALYSIS OF HEAT FLUX PARTITION IN SANDWICHED PLATES

Carolina P. Naveira-Cotta, cpncotta@hotmail.com
William Berk, billyberk@globo.com
Renato M. Cotta, cotta@mecanica.coppe.ufrj.br
Helcio R.B. Orlande, helcio@mecanica.coppe.ufrj.br
Laboratory of Transmission and Technology of Heat, LTTC
Mechanical Engineering Dept. – POLI & COPPE/UFRJ
Universidade Federal do Rio de Janeiro, Cx. Postal 68503
Cidade Universitária – Rio de Janeiro, RJ – 21945-970 – Brasil

Abstract. *The present work is aimed at demonstrating the use of infrared thermography and inverse problem analysis, in the identification of the required boundary conditions in a sandwiched plates configuration employed for thermophysical properties identification. The plates are heated at their contact with an electrical resistance of known dissipative power, and exchange heat by natural convection and radiation with the suroundings. Infrared camera measurements are taken at the external surface of one of the plates, while thermocouples are installed at the other plate external surface for validation purposes. Inverse analysis, provides the corresponding estimates of heat flux partition between the two plates. The present phase of tools construction and validation is essential for the reliable estimation of thermophysical properties in heterogeneous materials.*

Keywords*: Heat conduction, inverse problem, infrared thermography, heterogeneous media, conjugated problem.*

1. INTRODUCTION

Diffusion problems defined in heterogeneous media involve space variations of the physical properties in different forms, depending on the type of heterogeneity that prevails, such as large scale variations in functionally graded materials (FGM), abrupt variations in laminated media, and random variations due to fluctuations of local concentrations in dispersed systems, (Lin, 1992; Qiulin et al., 1999; Tavman & Akinci, 2000; Danes et al., 2003). In all such situations an accurate representation of the diffusion process requires a detailed local solution, generally associated with discrete numerical solutions with sufficiently refined meshes and significant computational effort, and/or semi-analytical approaches for specific or simplified functional forms of the diffusion equation coefficients, (Fudym et al., 2002; Naveira et al., 2008).

However, for the accurate determination of local variations in physical properties within heterogeneous media, one must seek an experimental technique that provides abundant information from spatially distributed measurements, in order to provide a firm basis for application of the appropriate inverse problem analysis. In addition, as the morphology of the medium directly influences the spatial behavior of the physical properties, it becomes critical not to disturb the structure along the experimental campaign by introducing intrusive sensors, such as thermocouples in the case of temperature measurements. Therefore, aimed at the identification of spatially variable thermophysical properties, the adoption of the non-intrusive technique of infrared thermography becomes of major interest, providing a large volume of measurements, both in space and time, and offering new perspectives towards the analysis of heat conduction in heterogeneous media, (Fudym, 2006; Fudym et al., 2007; Fudym et al., 2008).

Nevertheless, the inverse problem analysis for thermophysical properties determination in general requires the simultaneous estimation of usually unknown boundary conditions, in the form of boundary heat fluxes or heat transfer coefficients, which are to be estimated simultaneously with the parameters that define the properties. In other equally important situations, the boundary heat fluxes might have to be identified as the major task in the inverse analysis, when the properties are well known, but the heat transfer process involves conjugation of different modes, in the so called conjugated problems (Naveira et al., 2009; Lachi et al., 2008; Naveira-Cotta et al., 2009). The most interesting physical result that is obtained from the hybrid solution implemented in Naveira et al. (2009) for the conjugated conduction-convection problem, relates to the heat flux partition that occurs within the transient process and along the solid wall. For the experimental verification of both the proposed model and hybrid solution methodology, it was quite convenient to have an estimate of this heat flux partition function, determined by inverse analysis from temperature measurements at the fluid-solid interface along the plate (Lachi et al., 2008).

In this context, the present work is aimed at demonstrating the use of infrared thermography as a non-intrusive temperature measurement technique for boundary heat flux identification, together with the appropriate inverse problem analysis. The experimental-theoretical approach is applied in the identification of the heat flux partition between sandwiched thin plates heated at their common interface, and exchanging heat with the external environment through both natural convection and radiation. The infrared camera employed was the affordable and small *ThermoVision A-10* from *Flir Systems Inc*, which with dedicated data handling routines here developed, could be employed in quantitative thermographic analysis. The infrared camera measurements were taken at the external surface of one of the plates, while

thermocouples are installed at the other plate external surface for validation purposes. The inverse problem analysis is applied only to the plate with thermocouples, providing the corresponding estimates of heat flux partition between the two plates. The direct problem solution is then obtained with the estimated boundary conditions to predict the heat transfer behavior for the other plate, which is then compared to the infrared camera measurements. The thermography temperature data acquired by the camera in the form of digital level, are then treated by a computer code especially developed on the *Mathematica* 6.0 platform (Wolfram, 2005), that relates digital level to temperature values from temperature measurements provided by a reference thermocouple fixed at the same plate face.

2. EXPERIMENTAL APPARATUS AND PROCEDURE

The experimental setup presented in Figures 1a,b was designed and constructed for the present inverse heat transfer analysis, employing temperature measurements as obtained from the infrared camera *ThermoVision® Micron/A10* manufactured by *Indigo/Flir Systems* for wavelengths between 7.5 and 13.5 μm. The camera can withstand environment temperatures from -40 to 50C°, and is made of microbolometric detectors of vanadium oxide arranged in a 51 by 51 microns mesh. Two different setups were built, one for a horizontal plate arrangement, which is more evident in the left side of Fig.1a, and another one for a vertical plate configuration, shown in detail in Fig.1b, which is the experiment here reported.

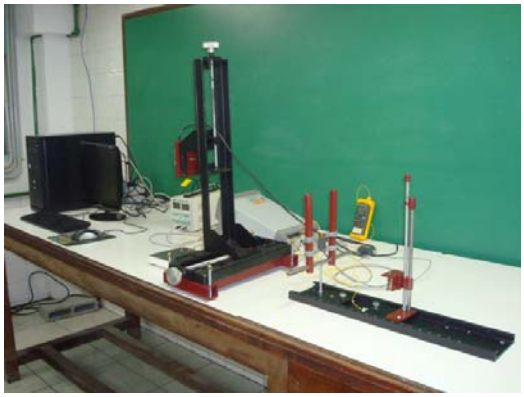

Fig. 1a. – General view of the experimental setup for the infrared thermography analysis

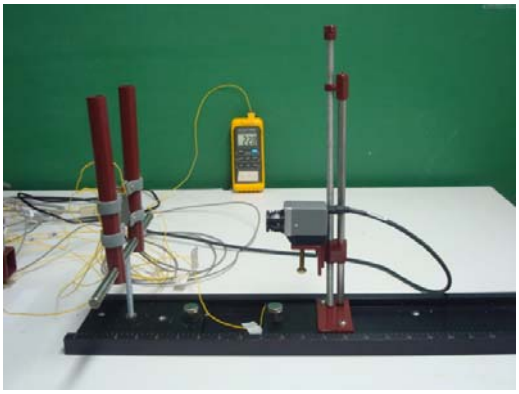

Fig. 1b. – Detail of the vertical plate setup, with the Thermovision A-10 camera installed facing the plate.

The vertical plate setup consists of two small plates of the same material (aluminum in the reported configuration), with the same thickness (3 mm) and lateral dimensions (4x4 cm). An electrical resistance (38.8 Ω), insulated with thin layers of Kapton tape, was employed in the heating of the two plates at their contact interface, with approximately the same lateral dimensions as of the two plates. The resistance is sandwiched between the two aluminum plates with the aid of a thermal compound paste and kept in place by screwed joints, as shown in Figure 2a. In other to further challenge the present heat flux partition analysis, the plate surface that faces the infrared camera was painted with a graphite ink, which brought its emissivity to around $\varepsilon = 0.97$, as stated by the manufacturer. A reference thermocouple (K type) was fixed at the top region of the plate surface that is directed towards the infrared camera (Fig. 2a). Five type K thermocouples were fixed to the plate surface opposite to the infrared camera, which was not covered by the high emissivity painting (Fig. 2b).

The experimental procedure was initiated by prescribing a voltage difference to be imposed on the electrical resistance, with a DC voltage regulator, first disconnected from the plates sandwich. The data acquisition was simultaneously started for the thermocouples and the infrared camera, and after a certain number of preliminary measurements to allow for averaging the initial conditions, the DC source switch is turned on to heat the two attached plates. The temperature increase could be followed through the computer monitoring, for both the thermocouples (Labview system) and thermography (Micron firmware) evolutions. Figures 3.a,b illustrate the images produced by the *TermoVision A-10* camera both at the moment the DC source is turned on, (Fig.3a), and after some elapsed heating time, when the heated plate image is much brighter, (Fig.3b). Once steady-state is achieved, the DC source is turned off. The thermocouples data and the acquired images were then identified and treated by the data analysis routine, constructed on the *Mathematica* 6.0 platform, that is described below.

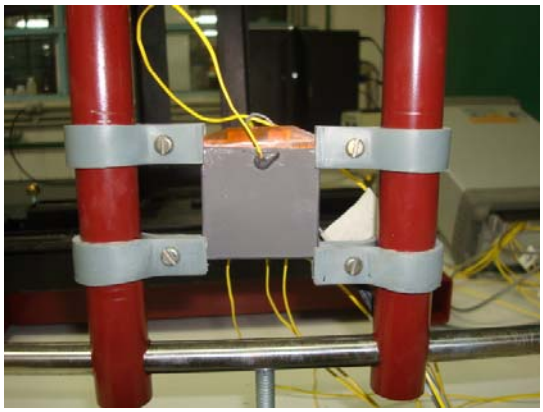

Fig. 2a – Detail of the plate surface and reference thermocouple that face the infrared camera.

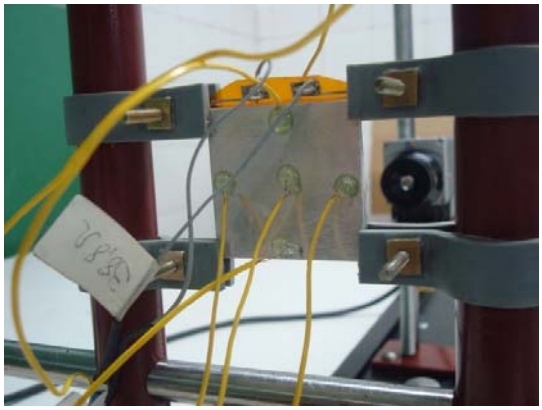

Fig. 2b – Detail of the plate surface opposite to the infrared camera, during fixation of thermocouples.

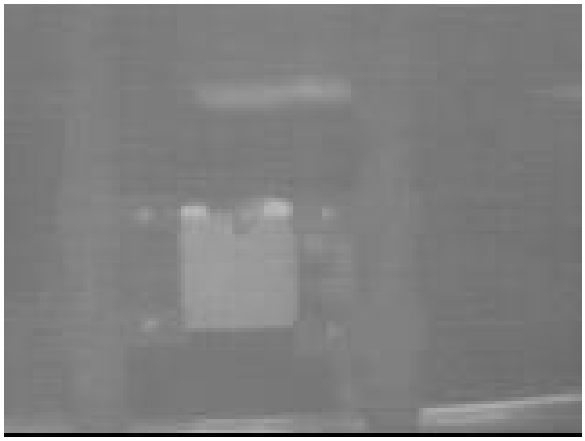

Fig. 3a – Infrared camera image acquired at the moment the DC source is switched on.

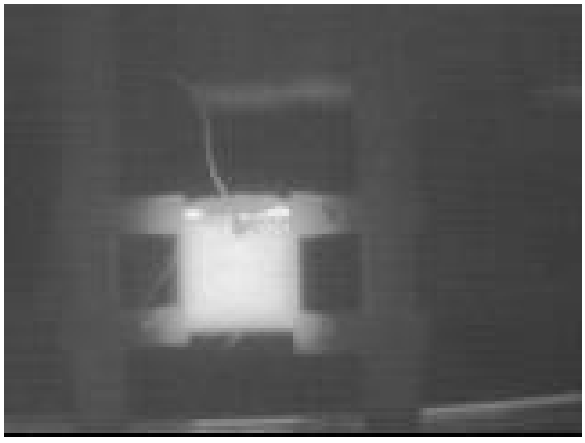

Fig. 3b - Infrared camera image acquired after some elapsed time during heating period.

3. DATA ANALYSIS

The *ThermoVision® A10* is a long-wavelength (7.5 – 13.5 microns) infrared camera, with a 164 (horizontal) x 128 (vertical) uncooled microbolometer sensor array of 51 x 51 micron pixels, designed for thermal imaging applications that demand minimum size, weight, and power consumption. The A10 provides advanced camera control through an RS-232 serial interface. This can be accessed using a PC with the standard serial communications port and the I/O Module. Included with the A10 is a PC-based Control Panel software (Micron Control Panel) that communicates with the camera, providing remote control of various camera features and modes as well as image capture using a graphical user interface (GUI). The acquisition system for the thermocouples is based on the modular system provided by Agilent Technologies (model 34970-A), which transfer data to the PC through the RS232 at a rate of 115 Kbits/s. The two acquisition procedures were interconnected and controlled via a Labview 7.0 dedicated routine.

The infrared camera images are saved on the jpeg format, and then imported by a *Mathematica* 6.0 notebook built with the purpose of treating the experimental data in general. The images are handled as "*digital level*" matrices, with values varying between -255 and 255. Since the A-10 is not a pre-defined radiometric camera, the information on *digital level* needs to be converted to temperature values. One possible approach is to use a reference temperature measurement at the active imaging field. Therefore, at the same physical point and time, both information on digital level and temperature, as provided by an installed thermocouple, are made available throughout the experiment, thus allowing for the correlation of such data. The starting point in constructing this correlation comes from the assumption that the microbolometer sensor provides a signal in *digital level* that is proportional to the radiative flux originated from each point at the plate that reaches the sensor, within the operational temperature range, that is, $DL \propto q_{cam}$. Assuming diffuse emission and surroundings reflection from an opaque gray surface, the radiation that originates from the plate surface is given as:

$$q_{rad}(x,y,t) = \varepsilon_{x,y}\sigma T^4(x,y,t) + \rho_{x,y}\sigma T_\infty^4 = \varepsilon_{x,y}\sigma T^4(x,y,t) + (1-\varepsilon_{x,y})\sigma T_\infty^4 \quad (1)$$

where the emissivity is allowed to be different at each position of the plate. For situations of large emissivities such as in the present situation of graphite painted surfaces, $\varepsilon_{x,y} \approx 0.97$, the contribution of the reflected radiation from the surroundings is in fact negligible, even at temperatures close to the external environment values. Nevertheless, it will be seen that the constructed correlation shall not require the local values of the emissivity, since a reference temperature measurement is being employed along the transient process.

The fraction of the total flux that leaves a surface element of the plate face and reaches the microbolometer sensor, is obtained from the knowledge of the associated view factor, and utilizing the corresponding reciprocity relation, the radiative flux that arrives at the camera is given by:

$$A_{cam}\, F_{cam-(x,y)} = A_{x,y}\, F_{(x,y)-cam} \quad (2)$$

$$q_{cam}(x,y,t) = \frac{A_{x,y}F_{(x,y)-cam}}{A_{cam}} q_{rad}(x,y,t) = F_{cam-(x,y)} q_{rad}(x,y,t) \quad (3)$$

The relation among the digital level at any position on the plate, the digital level at the reference position, and the respective radiative fluxes that reach the camera, i.e. in terms of temperatures in degrees Kelvin, can then be written as:

$$\frac{DL_{x,y}(t)}{DL_{ref}(t)} = \frac{F_{cam-(x,y)}\left(\varepsilon_{x,y}\sigma T^4(x,y,t) + (1-\varepsilon_{x,y})\sigma T_\infty^4\right)}{F_{cam-ref}\left(\varepsilon_{ref}\sigma T_{ref}^4(t) + (1-\varepsilon_{ref})\sigma T_\infty^4\right)} \quad (4a)$$

For the present situation of $\varepsilon_{x,y} \approx 1$, the reflected fraction may be disregarded, including the reference thermocouple region, yielding:

$$\frac{DL_{x,y}(t)}{DL_{ref}(t)} = \frac{F_{cam-(x,y)}\varepsilon_{x,y}T^4(x,y,t)}{F_{cam-ref}\varepsilon_{ref}T_{ref}^4(t)} \quad (4b)$$

Eq.(4b) may also provide a relation for the ratio of digital levels at the initial condition, t=0, when $T(x,y,t) \approx T_\infty$, from which the ratio of view factors and emissivities may be estimated:

$$\frac{DL_{x,y}(0)}{DL_{ref}(0)} = \frac{F_{(x,y)-cam}\varepsilon_{x,y}}{F_{ref-cam}\varepsilon_{ref}} \quad (5)$$

Before providing the final expression for the correlation between temperatures and digital levels, we have preferred to rewrite this result in terms of reduced digital level, thus eliminating eventual fluctuations of the initial conditions due to the external environment variations. Essentially we performed a subtraction of each image by that corresponding to the initial state, throughout the transient experiment, and thus enhancing the image of greater interest. The reduced digital level is thus proportional to the reduced incident radiative flux at the camera:

$$DLS \propto q_{cam}(x,y,t) - q_{cam}(x,y,0) \quad (6)$$

Then, eq(4b) is rewritten for the filtered digital level, in the form:

$$\frac{DLS_{x,y}(t)}{DLS_{ref}(t)} = \frac{F_{cam-(x,y)}\varepsilon_{x,y}\left(T^4(x,y,t) - T_\infty^4\right)}{F_{cam-ref}\varepsilon_{ref}\left(T_{ref}^4(t) - T_\infty^4\right)} \quad (7a)$$

Making use of eq.(5), the view factors and emissivities are eliminated, providing:

$$\frac{DLS_{x,y}(t)}{DLS_{ref}(t)} = \frac{DL_{x,y}(0)}{DL_{ref}(0)} \frac{\left(T^4(x,y,t) - T_\infty^4\right)}{\left(T_{ref}^4(t) - T_\infty^4\right)} \tag{7b}$$

We then reach the final working expression for converting digital levels and the reference temperature measurements, into the local temperature values at each position of the plate, given by:

$$T(x,y,t) = \sqrt[4]{\frac{DLS_{x,y}(t)DL_{ref}(0)}{DLS_{ref}(t)DL_{x,y}(0)}\left(T_{ref}^4(t) - T_\infty^4\right) + T_\infty^4} \tag{8}$$

The temperature cartography is then automatically constructed by the *Mathematica* routine, by taking the digital values for each position as the average of the four adjacent pixels values.

4. DIRECT AND INVERSE PROBLEM ANALYSIS

Assuming negligible temperature gradients within the two metallic thin plates, in light of the low values of the effective Biot numbers and small vertical variation of the heat transfer coefficients along these small plates, the global energy balance at one of the plates, for constant thermophysical properties, is written in terms of the average temperature temporal variation as:

$$\rho c_p L_z \frac{dT_m(t)}{dt} = h\left(T_\infty - T_m(t)\right) + \varepsilon\sigma\left(T_\infty^4 - T_m^4(t)\right) + f(t)q_w, \qquad t > 0 \tag{9a}$$

$$T_m(0) = T_\infty \tag{9b}$$

where the heat flux partition function is parametrized as:

$$f(t) = d\exp[-bt] + c \tag{10}$$

For a purely convective cooling and a constant heat transfer coefficient, the temporal behavior of the heat flux should follow that of the temperature itself, and for this reason the heat flux partition, "*f(t)*", was written according to eq.(10) above. Thus, we seek the estimation of the parameters in eq.(10) from the averaged thermocouple measurements at the plate surface along the transient. Therefore, it is assumed that the power dissipated at the electrical resistance is partitioned between the two sandwiched plates, yielding the two heat fluxes below at each plate surface:

$$q_{w1}(t) = f(t)q_w \tag{11a}$$

$$q_{w2}(t) = (1 - f(t))q_w \tag{11b}$$

Problem (9) may be readily solved by numerical means, for instance through function **NDSolve** in the *Mathematica* system (Wolfram, 2005). Also of interest, is the linearized version of the present problem, by factoring the radiation flux expression and producing an approximate radiation heat transfer coefficient, as:

$$q_{rad}(t) \cong h_r\left(T_m(t) - T_\infty\right), \quad where \quad h_r = 4\varepsilon\sigma T_\infty^3 \tag{12}$$

which then results in the linear ODE below, in terms of the effective heat transfer coefficient (h_{ef}=h+h_r):

$$\rho c_p L_z \frac{dT_m(t)}{dt} = h_{ef}\left(T_\infty - T_m(t)\right) + f(t)q_w, \qquad t > 0 \tag{13a}$$

$$T_m(0) = T_{amb} \tag{13b}$$

The simplified linear formulation (13) provides the following useful exact solution:

$$T_{m,L}(t) = T_\infty + \frac{q_w}{\rho c_p L_z}\int_0^t f(t')e^{-\frac{h_{ef}}{\rho c_p L_z}(t-t')}dt' \tag{14}$$

Inverse problems may be solved as parameter or function estimations. If some information on the functional form of the unknown is available, the inverse problem is in general simplified to the estimation of a few unknown parameters. However, if no information is a priori available, the inverse problem is considered a function estimation approach. For the heat flux function with time dependence to be estimated in the present work, for which some information is in principle available, a possible representation is provided by eq.(10).

Consider the vector of parameters appearing in the physical model formulation as

$$\mathbf{P}^T \equiv [P_1, P_2, ..., P_N] \tag{15}$$

where N is the number of parameters. For the estimation of such parameters, we consider in the general case that the following vector of measured temperatures is available:

$$\mathbf{Y}^T = \left(\vec{Y}_1 , \vec{Y}_2 , \ldots , \vec{Y}_I \right) \tag{16}$$

where $\vec{Y}_i$ contains the measured temperatures for each of the S sensors at time t_i, $i = 1, \ldots, I$, that is,

$$\vec{Y}_i = \left(Y_{i1} , Y_{i2} , \ldots , Y_{iS} \right) \quad \text{for } i=1,\ldots,I \tag{17}$$

In this work, the following statistical hypotheses regarding the measurements are assumed valid (Beck and Arnold, 1977): the errors in the measured variables are additive, uncorrelated, normally distributed, with zero mean and known constant standard-deviation; only the measured variables appearing in the objective function contain errors; and there is no prior information regarding the values and uncertainties of the unknown parameters. In this case, the likelihood function can be expressed as (Beck and Arnold, 1977, Kaipio and Sommersallo, 2005):

$$\pi(\mathbf{Y}|\mathbf{P}) = (2\pi)^{-M/2} \left| \mathbf{W}^{-1} \right|^{-1/2} \exp\left[-\frac{1}{2} [\mathbf{Y} - \mathbf{T}(\mathbf{P})]^T \mathbf{W} [\mathbf{Y} - \mathbf{T}(\mathbf{P})] \right] \tag{18}$$

where ($M = S\ I$) is the number of measurements and W is the inverse of the covariance matrix of the measurement errors.

For uncorrelated measurements:

$$\mathbf{W} = \begin{bmatrix} 1/\sigma_1^2 & & & 0 \\ & 1/\sigma_2^2 & & \\ & & \ddots & \\ 0 & & & 1/\sigma_M^2 \end{bmatrix} \tag{19}$$

where σ_i is the standard-deviation of the measurement Y_i, $i = 1, \ldots, M$.

From equation (18) it can be noticed that, with the statistical hypotheses listed above, maximum likelihood estimates can be obtained through the minimization of the following objective function:

$$S_{ML}(\mathbf{P}) = \left[\mathbf{Y} - \mathbf{T}(\mathbf{P}) \right]^T \mathbf{W} \left[\mathbf{Y} - \mathbf{T}(\mathbf{P}) \right] \tag{20}$$

In this work, we make use of the Levenberg-Marquardt method for the minimization of the maximum likelihood objective function given by equation (20). The iterative procedure of such method can be written as:

$$\mathbf{P}^{k+1} = \mathbf{P}^k + [\mathbf{J}^T \mathbf{W} \mathbf{J} + \lambda^k \boldsymbol{\Omega}^k]^{-1} \mathbf{J}^T \mathbf{W} [\mathbf{Y} - \mathbf{T}(\mathbf{P}^k)] \tag{21}$$

where k denotes the number of iterations, $\mathbf{J}$ is the sensitivity matrix, $\boldsymbol{\Omega}$ is a diagonal matrix and λ is a scalar named damping parameter (Beck and Arnold, 1977, Ozisik and Orlande, 2000). The purpose of the matrix term $\lambda^k \boldsymbol{\Omega}^k$ in equation (21) is to damp oscillations and instabilities due to the ill-conditioned character of the problem, by making its components large as compared to those of $\mathbf{J}^T\mathbf{W}\mathbf{J}$, if necessary. The damping parameter is made large in the beginning of the iterations. With such an approach, the matrix $\mathbf{J}^T\mathbf{W}\mathbf{J}$ is not required to be non-singular in the beginning of iterations and the Levenberg-Marquardt Method tends to the Steepest Descent Method, that is, a very small step is taken in the negative gradient direction. The parameter λ^k is then gradually reduced as the iteration procedure advances to the solution of the parameter estimation problem and then the Levenberg-Marquardt Method tends to the Gauss Method

(Beck and Arnold, 1977). However, if the errors inherent to the measured data are amplified generating instabilities on the solution, as a result of the ill-conditioned character of the problem, the damping parameter is automatically increased. Such an automatic control of the damping parameter makes the Levenberg-Marquardt method a quite robust and stable estimation procedure (Ozisik and Orlande, 2000).

5. RESULTS AND DISCUSSION

Figures 4.a,b identify the position of the thermocouples in the present experiment, including the reference thermocouple tp1 installed in the surface that faces the infrared camera, and other five sensors (tp2 to tp6), that have been employed to obtain the average surface temperature employed in the inverse problem analysis. A few results are here reported, chosen from a large collection of tests that have been performed, for the specific situation of an applied voltage of 8V after 300 sec that the acquisition is initiated, with both the camera and thermocouples readings being performed at every 10 sec.

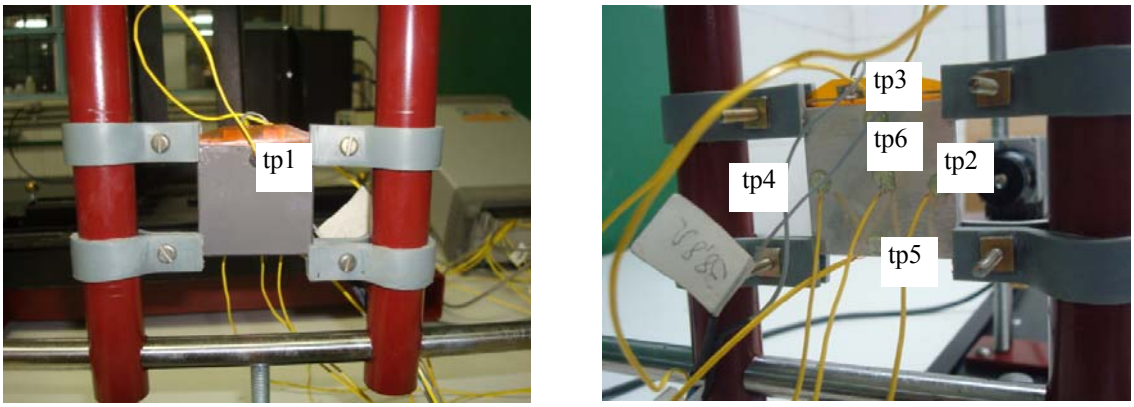

(a) **(b)**

Fig.4a, b – Position of the thermocouples for the vertical plates experiment.

Figures 5a,b illustrate the measurements, the three thermocouples vertically aligned along the plate surface opposite to the camera, and the measurements of the two thermocouples positioned at the top at both surfaces of the plates, respectively. It can be noticed that the three thermocouples vertically positioned on the plate face have practically the same values, with the steady state temperatures around 55 C, which confirms the assumption that the heat transfer coefficient variation along the vertical direction is not negligible. Figure 5b shows that the measurements of the two thermocouples located at the top positions of each plate differ more significantly, mainly due to the fairly different emissivities of the two surfaces (no painting, $\varepsilon \approx 0.10$) and (graphite painting, $\varepsilon \approx 0.97$). This fact induces an asymmetry to the heat flux partition. And, as expected, the temperatures on the plate with larger emissivity (tp1) has consistently lower values than the other one (tp3). Figures 6a,b show the two sets of data that have been employed in the correlation of digital level and temperatures (here in degrees Celsius). Fig.6a refers to the tp1 thermocouple while Fig.6b corresponds to the filtered digital level at the tp1 thermocouple region, averaged in four adjacent pixels. Once the conversion is interpolated, according to eq. (8), it can be applied to the whole plate surface. It should be noted that the initial period of 300 sec was already removed from these figures.

Next, the averaged values of the five thermocouple readings at the face opposite to the camera were utilized to estimate the coefficients in the heat flux partition function, eq. (10). Then, the estimated values were employed to reconstruct the heat flux to the other plate, with large emissivity, so as to predict the temperature evolution at this plate that was monitored by the infrared camera. The estimates that are now shown were obtained through the Levenberg-Marquardt algorithm implemented on the *FindMinimum* function of *Mathematica* 6.0. It has been observed that for the case of a low emissivity plate, such as the one opposite to the camera, not covered by the graphite painting, there is not a major difference between the predictions of the nonlinear and linearized models. Most important was the simultaneous estimation of the effective heat transfer coefficient and the thermal capacitance as is next illustrated. We have first employed the nonlinear model to estimate the three coefficients b, c, and d, from correlation and literature values for the convective heat transfer coefficient and for the aluminum plate thermal capacitance. We have then considered the emissivity to be (ε=0.1), the thermal capacitance (ρc_p=2.45*10^6 J/m^3°C), the average natural convection heat transfer coefficient, h_m=12.32 W/m^2°C, while the average radiation heat transfer coefficient was estimated as h_r= 0.5833 W/m^2°C. From the values obtained for the three coefficients in the partition function (d=0.209 W/m^2, b=0.00233 s^{-1}, c=0.403 W/m^2), the steady state situation leads to around 40% heat flux partition to the unpainted surface, and around 60% for the graphite painted surface. Then, the inverse problem analysis was repeated, but now including the effective heat transfer coefficient and the aluminum thermal capacitance in the list of parameters to be estimated, yielding the final estimated values (d=0.112 W/m^2, b=0.00210 s^{-1}, c=0.405 W/m^2, h_{ef}=13.07 W/m^2°C, ρc_p=2.07x10^6 J/m^3°C).

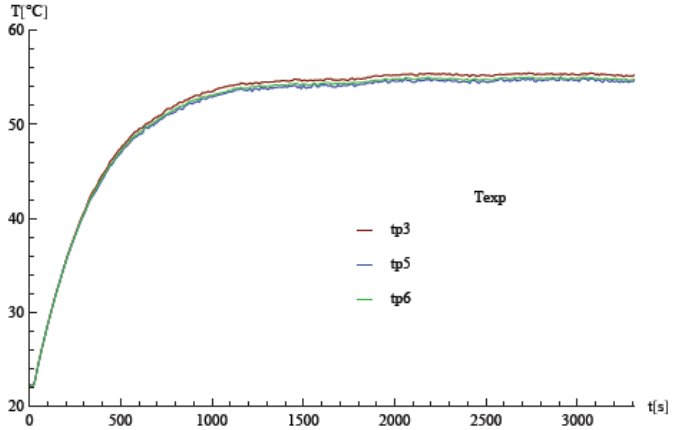

Figure 5.a – Temperatures of thermocouples *tp5, tp6 e tp3* vertically aligned on the plate surface opposite to the camera.

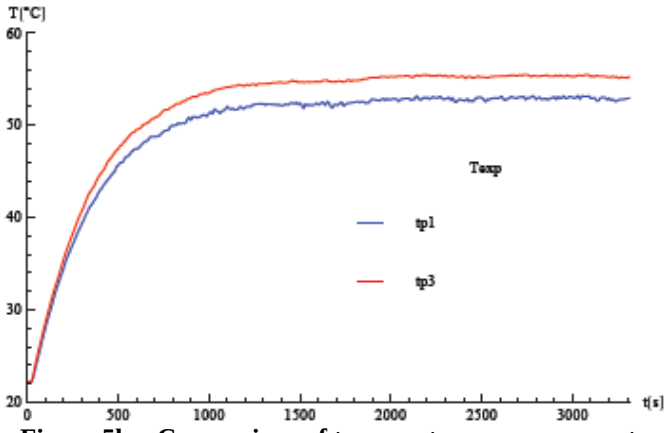

Figure 5b – Comparison of temperature measurements from the two thermocouples located at the top of the two plates.

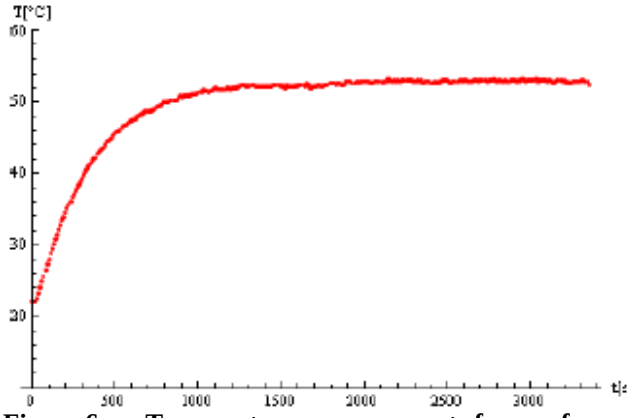

Figure 6.a – Temperature measurements from reference thermocouple *tp1*.

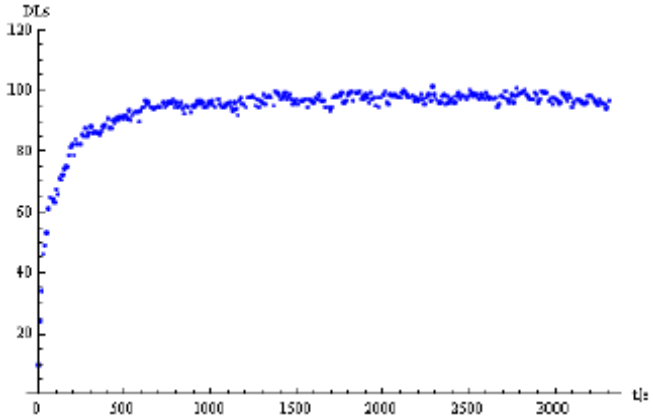

Figure 6.b – *Digital level* after filtering, at the reference thermocouple region.

Figure 7 illustrates the two estimated partition functions as described above, the first one (blue curve) employing literature values for the heat transfer coefficient and the thermal capacitance, and the second one (red curve) estimating simultaneously the heat flux partition coefficients and these two quantities and the black curve represents the steady state heat flux partition to the uncovered surface (around 40%). It can be noticed that although the steady-state behavior is quite similar, the initial transient shows some differences when the effective heat transfer coefficient and thermal capacitance are also estimated instead of deterministically fixed.

These five estimated parameters are now employed for providing theoretical predictions for comparison purposes. Figures 8a-d show the excellent agreement between theoretical and experimental temperature, as obtained for four thermocouple positions, *tp5* (a), *tp6* (b), *tp3* (c), and *tp1* (d), by employing the five estimated parameters, including the reference thermocouple measurements, tp1, on the graphite covered surface.

Once the heat flux partition has been identified, we may also compare the theoretical predictions to the thermography measurements available for the graphite covered plate surface. Figures 9a,b illustrate such a comparison for two positions, corresponding to the thermocouple positions *tp6* (a) e *tp3* (b) on the graphite painted plate. The agreement is indeed fairly good, in light of the simplicity of the model here employed. Also, it should be noted that this comparison is not an analysis of the residues such as the previous one, but rather an independent verification of the model and the estimated parameters values through a different set of experimental results, obtained via a different experimental approach on the other side of the plate.

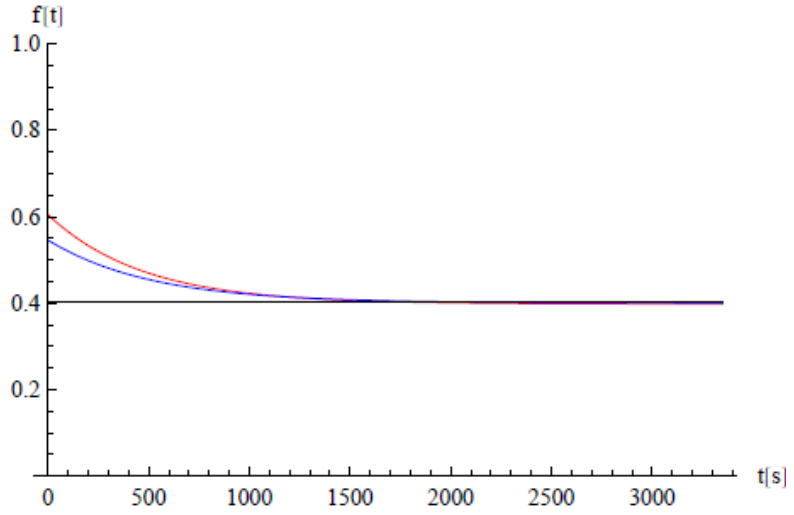

Figure 7 – Estimated heat flux partition functions for three unknown parameters (*d*, *b*, and *c*) - blue curve, and five unknown parameters (*d*, *b*, *c*, h_{ef}, and ρc_p) - red curve. Steady state heat flux partition for the surface without graphite painting - black curve

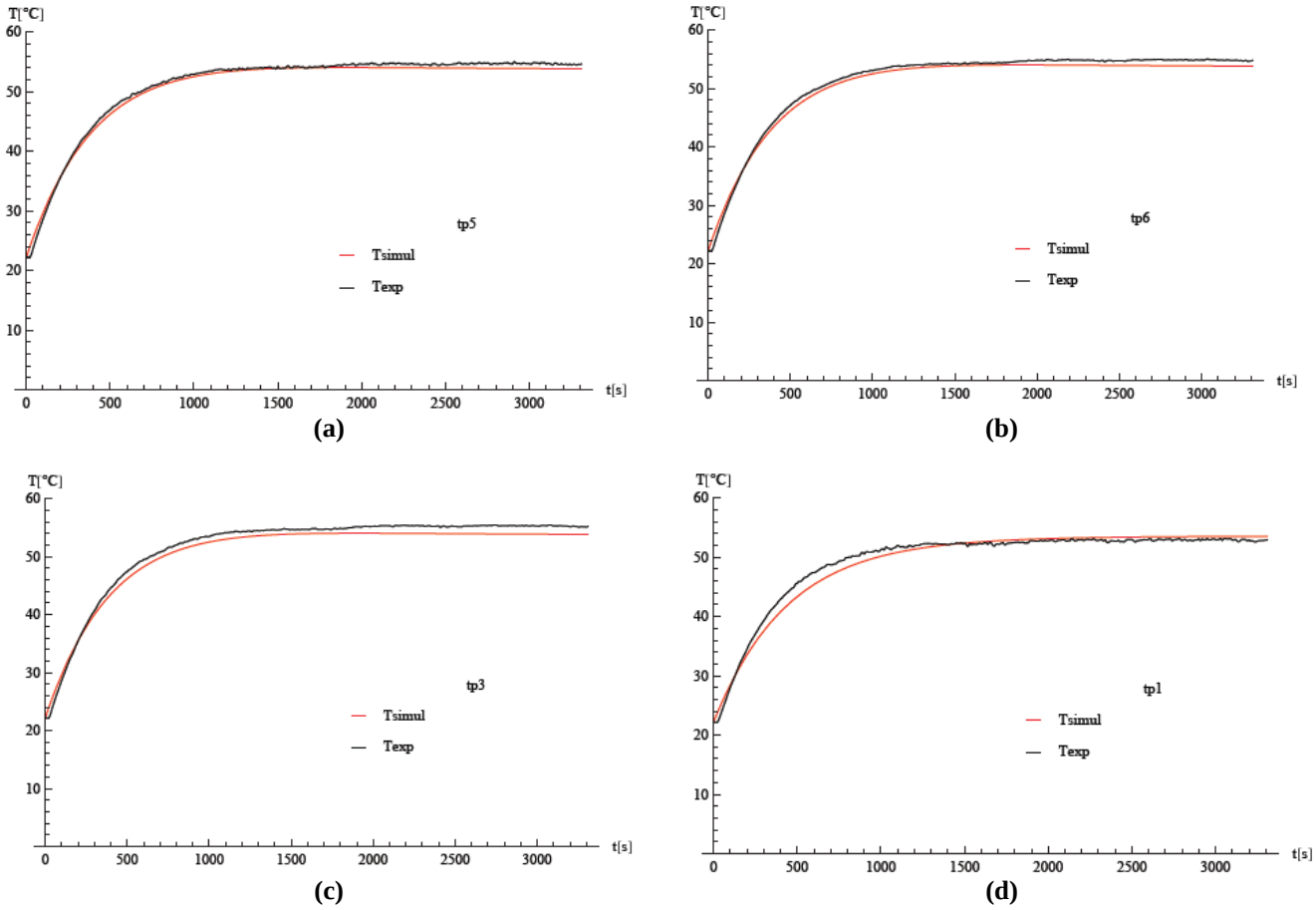

Figures 8a-d– Comparison of experimental (black curve) and simulated temperatures (red curve) at four different thermocouple positions: *tp5* (a), *tp6* (b), *tp3* (c), and *tp1* (d) with five parameters estimated.

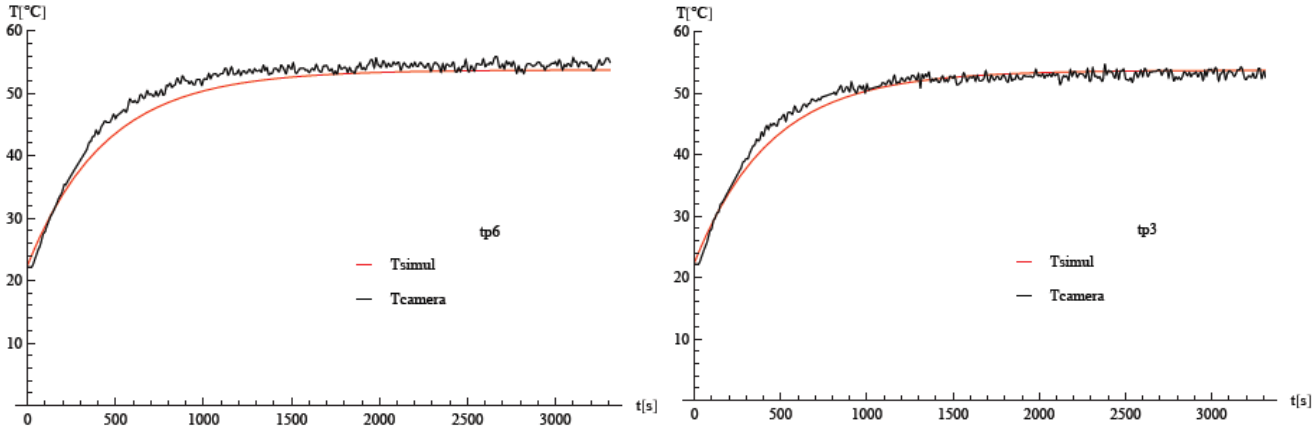

Figures 9a,b – Comparison of theoretical (red curve) and experimental (thermography-black curve) values at positions corresponding to the thermocouple positions *tp6* (a) e *tp3* (b) on the graphite painted plate.

The present analysis in concluded by providing a comparison of theoretical and experimental (thermography) results for the averaged temperature evolutions on the graphite painted surface, first by considering the average over the whole 22x22 pixels matrix, Fig.10a, which compare sthe theoretical temperatures employing the five estimated parameters and the thermography experimental results averaged at the whole plate. Fig.10b also compares the theoretical temperatures employing the five estimated parameters, but with the thermography temperatures values averaged only over the five positions corresponding to the same thermocouple positions as on the opposite plate (*tp2*, *tp3*, *tp4*, and *tp5*). An improved agreement is now observed after the lumping procedure is performed over the thermography experimental data, confirming the adequacy of the model adopted, of the parameters estimation procedure, and also confirming the thermographic instrumentation developed.

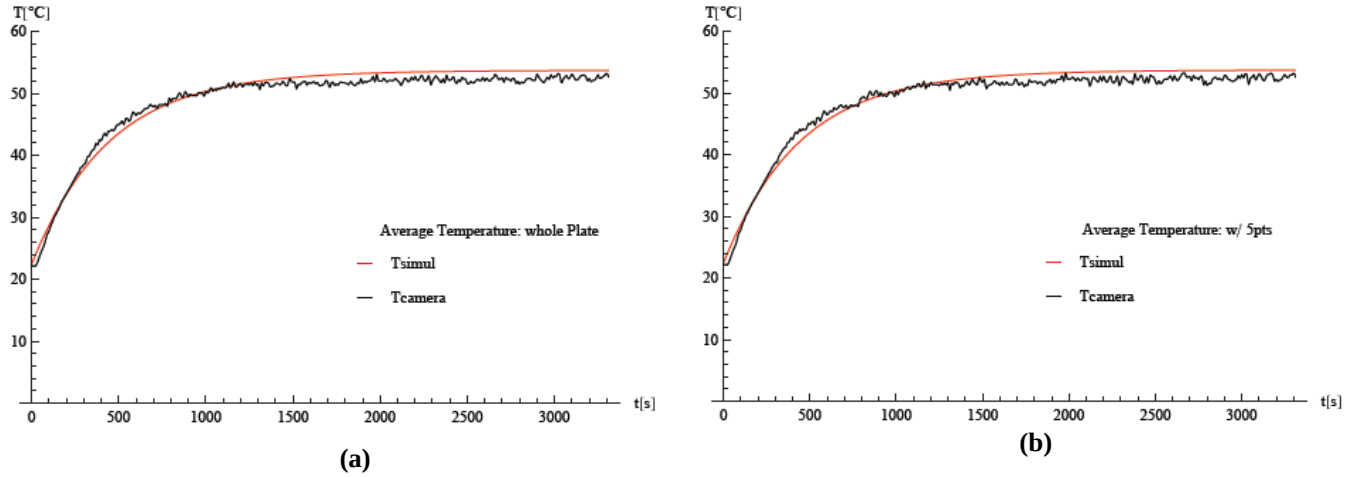

Figures 10a,b – Comparison of theoretical and experimental (thermography) results for space averaged temperatues at the graphite painted plate: (a)average at whole plate, (b)average for just five points corresponding to the same positions as on opposite plate.

6. ACKNOWLEDGEMENTS

The authors would like to acknowledge the financial support provided by CNPq, Brasil, and CNRS, France, and the assistance and helpful discussions in the technical visit of Dr. Christophe Pradère (ENSAM/Bordeaux) to COPPE/UFRJ.

7. REFERENCES

Beck, J. and Arnold, K., (1977), Parameter Estimation in Engineering and Science, Wiley Interscience, New York.

Danes, F., Garnier, B., and Dupuis, T. (2003), "Predicting. Measuring and Tailoring the Transverse Thermal Conductivity of Composites from Polymer Matrix and Metal Filler", Int. J. of Thermophysics, Vol.24, pp. 771-784.

Fudym, O., Ladevie, B., and Batsale, J.C. (2002), "A Seminumerical Approach for Heat Diffusion in Heterogeneous Media: One Extension of the Analytical Quadrupole Method", Num. Heat Transfer, Part B: Fundamentals, Vol.42, pp. 325-348.

Fudym, O. (2006), "Velocity and heat transfer parameters mapping: thermal quadrupoles and infrared image processing", 11th Brazilian Congress of Thermal Sciences and Engineering – ENCIT, Curitiba – Brazil, Dec. 5-8.

Fudym,O., Batsale, J.C., Battaglia, J.L. (2007), "Thermophysical properties mapping in semi-infinite longitudinally cracked plates by temperature image processing", Inverse Problems in Science and Engineering, Vol.15, No.2, pp.163-176.

Fudym, O., Orlande, H.R.B., Bamford, M., and Batsale, J.C. (2008), "Bayesian Approach for Thermal Diffusivity Mapping from Infrared Images Processing with Spatially Random Heat Pulse Heating", 6th ICIPE Proceedings, 6th Int. Conf. on Inverse Problems in Engineering: Theory and Practice, Dourdan, France, June 15th-19th.

Kaipio, J. and Somersalo, E., (2005),Statistical and Computational Inverse Problems, Springer, New York.

Lachi, M., Naveira, C. P., Orlande, H.R.B., and Cotta, R.M. (2008), "Inverse Problem Analysis for Heat Flux Estimation in Conjugated Conduction-External Convection", Proc. of the 4th Int. Symposium on Advances in Computational Heat Transfer, CHT-08, Marrakesh, Morocco, May.

Lin, S.H. (1992), "Transient Conduction in Heterogeneous Media", Int. Comm. Heat & Mass Transfer, Vol.10, pp.165-174.

Naveira, C.P., Fudym, O., Cotta, R.M., and Orlande, H.R.B. (2008), "Integral Transform Solutions for Diffusion in Heterogeneous Media", Proceedings of IMECE2008, ASME International Mechanical Engineering Congress & Exposition, Paper no. IMECE2008-69114, Boston, MA, USA, November 1-6.

Naveira, C.P., Lachi, M., Cotta, R.M., and Padet, J. (2009), "Hybrid Formulation and Solution for Transient Conjugated Conduction-External Convection", Int. J. Heat and Mass Transfer, Vol. 52, No. 1-2, pp. 112-123.

Naveira-Cotta, C.P., Lachi, M., Rebay, M., and Cotta, R.M. (2009), "Comparison of Experiments and Hybrid Simulations of Transient Conjugated Conduction-Convection-Radiation", ICCHMT International Symposium on Convective Heat and Mass Transfer in Sustainable Energy, CONV-09, Yasmine Hammamet, Tunisia, April.

Qiulin, F. Xingcheng, X., Xingfang, H., Jingkun, G. (1999), "Calculating Method of the Equivalent Thermal Conductivity of Functionally Gradient Materials", Materials Science & Eng., Vol.A261, pp.84-88.

Ozisik, M.N. and Orlande, H.R.B. (2000) *Inverse Heat Transfer: Fundamentals and Applications*, Taylor and Francis, New York.

Schwaab, M. & Pinto, J.C. (2007), Análise de Dados Experimentais I: Fundamentos de Estatística e Estimação de Parâmetros, Editora E-Papers, Rio de Janeiro.

Tavman, I.H., and Akinci, H. (2000), "Transverse Thermal Conductivity o Fiber Reinforced Polymer Composites", Int. Comm. Heat & Mass Transfer, Vol.27, pp.253-261.

8. RESPONSIBILITY NOTICE

The authors are the only responsible for the printed material included in this paper.